blood

2011 117: 39-48
Prepublished online Nov 1, 2010;
doi:10.1182/blood-2010-09-307595

Detection and isolation of cell-derived microparticles are compromised by protein complexes resulting from shared biophysical parameters

Bence György, Károly Módos, Éva Pállinger, Krisztina Pálóczi, Mária Pásztói, Petra Misják, Mária A. Deli, Áron Sipos, Anikó Szalai, István Voszka, Anna Polgár, Kálmán Tóth, Mária Csete, György Nagy, Steffen Gay, András Falus, Ágnes Kittel and Edit I. Buzás

Blood (print ISSN 0006-4971, online ISSN 1528-0020), is published weekly by the American Society of Hematology, 2021 L St, NW, Suite 900, Washington DC 20036.

e-*Blood*

Detection and isolation of cell-derived microparticles are compromised by protein complexes resulting from shared biophysical parameters

Bence György,[1] Károly Módos,[2] Éva Pállinger,[1] Krisztina Pálóczi,[1] Mária Pásztói,[1,3] Petra Misják,[1] Mária A. Deli,[4] Áron Sipos,[5] Anikó Szalai,[5] István Voszka,[2] Anna Polgár,[6] Kálmán Tóth,[7] Mária Csete,[5] György Nagy,[1,8] Steffen Gay,[9] András Falus,[1,3] *Ágnes Kittel,[10] and *Edit I. Buzás[1]

[1]Department of Genetics, Cell- and Immunobiology, Semmelweis University, Budapest, Hungary; [2]Department of Biophysics and Radiation Biology, Semmelweis University, Budapest, Hungary; [3]Research Group for Inflammation Biology and Immunogenomics, Hungarian Academy of Sciences, Budapest, Hungary; [4]Laboratory of Molecular Neurobiology, Institute of Biophysics, Biological Research Center of the Hungarian Academy of Sciences, Szeged, Hungary; [5]Department of Optics and Quantum Electronics, University of Szeged, Szeged, Hungary; [6]National Institute of Rheumatology and Physiotherapy, Budapest, Hungary; [7]Department of Orthopaedics, University of Szeged, Szeged, Hungary; [8]Department of Rheumatology, Semmelweis University, Budapest, Hungary; [9]Center for Experimental Rheumatology, Zürich Center for Integrative Human Physiology, USZ, Zürich, Switzerland; and [10]Institute of Experimental Medicine, Hungarian Academy of Sciences, Budapest, Hungary

Numerous diseases, recently reported to associate with elevated microvesicle/microparticle (MP) counts, have also long been known to be characterized by accelerated immune complex (IC) formation. The goal of this study was to investigate the potential overlap between parameters of protein complexes (eg, ICs or avidin-biotin complexes) and MPs, which might perturb detection and/or isolation of MPs. In this work, after comprehensive characterization of MPs by electron microscopy, atomic force microscopy, dynamic light-scattering analysis, and flow cytometry, for the first time, we drive attention to the fact that protein complexes, especially insoluble ICs, overlap in biophysical properties (size, light scattering, and sedimentation) with MPs. This, in turn, affects MP quantification by flow cytometry and purification by differential centrifugation, especially in diseases in which IC formation is common, including not only autoimmune diseases, but also hematologic disorders, infections, and cancer. These data may necessitate reevaluation of certain published data on patient-derived MPs and contribute to correct the clinical laboratory assessment of the presence and biologic functions of MPs in health and disease. (*Blood*. 2011;117(4):e39-e48)

Introduction

Membrane vesicles are small subcellular structures surrounded by a phospholipid bilayer. Their release by various cell types is enhanced during activation and apoptosis.[1] They represent heterogeneous structures and can be classified into several groups depending on their size, antigenic features, and mechanism of cellular release.[1] The two best characterized categories include exosomes and microvesicles/microparticles (MPs). Both populations are characterized by the exposure of phosphatidylserine, which allows annexin-V (AX) to bind to these–lipid surfaces.[1] Exosomes are composed of small, 50- to 100-nm–sized structures released on exocytosis of multivesicular bodies.[1] The diameter of MPs, formed by membrane blebbing, is described to be 100 to 1000 nm[2]. However, precise definitions of MPs are still lacking.[1,2] MPs are found in various biologic fluids, including blood plasma,[3] urine,[4] and synovial fluid (SF).[5,6] Numerous flow cytometry (FC) studies using blood plasma have shown correlation of MP counts with human cardiovascular[7] and autoimmune diseases,[8] hematologic disorders,[9] and cancer.[10] Of particular interest, autoimmune diseases were reported to be characterized by elevated levels of MPs.[11]

The assessment of exosomes and MPs is complicated by the presence of further known categories of membrane bound subcellular structures, such as apoptotic vesicles, exosome-like vesicles, membrane particles, and ectosomes.[1] There is a substantial size overlap among the aforementioned vesicle categories, and the size distribution of a given vesicle preparation may also be affected by the method used for their isolation.[3,12,13] Recently, attempts have been made to standardize isolation and detection protocols for membrane vesicles.[3,14] Up until now, no systematic study has been carried out concerning MP size distributions in blood plasma and SF.

In contrast to membrane vesicles, immune complexes (ICs) have been known for a long time and were characterized extensively by immunologists. ICs consist of multivalent antigens and antibodies and are either soluble or insoluble.[15] Soluble ICs consist of 2 to 10 macromolecules, whereas insoluble ICs form colloidal precipitates.[15] In the presence of a given antigen/antibody ratio, temperature, ionic strength, and pH, soluble ICs lose their solubility. Insoluble IC particles are characterized by significant light scattering and visible turbidity.[15] ICs are well documented to have immunoregulatory and immunopathologic functions.[16,17] In our work, we chose to investigate rheumatoid arthritis (RA) SF samples reported to contain high amounts of ICs.[17]

In this study, we demonstrated overlapping biophysical properties (size, light scattering, sedimentation) of protein complexes

Submitted September 21, 2010; accepted October 19, 2010. Prepublished online as *Blood* First Edition paper, November 1, 2010; DOI 10.1182/blood-2010-09-307595.

*Á.K. and E.I.B. contributed equally to this study.

An Inside *Blood* analysis of this article appears at the front of this issue.

The online version of this article contains a data supplement.

The publication costs of this article were defrayed in part by page charge payment. Therefore, and solely to indicate this fact, this article is hereby marked "advertisement" in accordance with 18 USC section 1734.

with MPs. Our observations may have an impact of MP assessment in a broad variety of diseases in which IC formation is common.[17-23]

Methods

Patients

Normal human blood plasma was collected from healthy donors (4 females, 1 male; mean age ± SD, 38.2 ± 13.6 years; age range, 25-50 years). Blood plasma was also tested from RA patients (9 females, 2 males; mean age ± SD, 61.8 ± 11.7 years; age range, 38-76 years) and from patients with osteoarthritis (OA) (10 females; mean age ± SD, 58.4 ± 14.7 years; age range, 35-75 years). SF samples from patients with RA (11 females, 1 male; mean age ± SD, 56.2 ± 15.4 years; age range, 25-74 years) and OA (10 females, 2 males; mean age ± SD, 61.7 ± 6.4 years; age range, 50-68 years) were included in this study. All RA patients fulfilled the diagnostic criteria of the American College of Rheumatology.[24] Patients were treated in the Department of Rheumatology, Semmelweis University (Budapest, Hungary), the National Institute of Rheumatology and Physiotherapy (Budapest), and the Department of Orthopaedics, University of Szeged (Szeged, Hungary). Plasma and SF were centrifuged at 250*g* for 10 minutes and 650*g* for 20 minutes, respectively, to eliminate cells. Aliquots of the samples were stored at −20°C until use. During the entire investigation period, we followed the guidelines and regulations of the Helsinki Declaration in 1975, and the experiments were approved by the Hungarian Scientific and Research Ethics Committee; all patients signed an informed consent form.

Microparticle isolation

MPs were isolated from blood plasma and SF. SF samples were digested with 10 U/mL sheep testis hyaluronidase (Sigma-Aldrich) for 30 minutes at 37°C. Platelets, cell debris, and larger apoptotic bodies were pelleted for 10 minutes at 3000*g*, followed by filtration through an 800 nm filter (Millipore) by gravity. MPs were sedimented as described previously (20 500*g*, 60 minutes at room temperature).[25,26]

Isolation of ICs

ICs were isolated from SF samples of patients with RA. Cell-depleted SFs (2 mL) were applied onto antihuman IgG and antihuman IgM agarose columns in 0.01M sodium phosphate buffer containing 0.15M NaCl, pH 7. After 2-hour incubation at room temperature, the column was washed with 50 times volumes of binding buffer. The elution of the bound proteins was carried out using 4M $MgCl_2$ buffer (pH 5.5). Eluted ICs were dialyzed against phosphate-buffered saline (PBS) overnight. IC preparations were stained with antihuman IgG-fluorescein isothiocyanate (FITC), antihuman IgM-FITC (Sigma-Aldrich), and AX-FITC (BD Biosciences) to exclude the presence of MPs.

Generation of protein complexes

Artificial ICs were generated by mixing antigens with specific antibodies using different ratios. Human lactoferrine (LF), antihuman LF, ovalbumin (OVA), and antihuman OVA were purchased from Sigma-Aldrich. Mouse IgM was produced by the HFPG-846 hybridoma,[27] and antimouse IgM-FITC was purchased from Sigma-Aldrich. Antigens and antibodies were mixed in 50 μL PBS using different ratios (from 1:10 000 to 10 000:1). Samples were diluted up to 300 μL in PBS and were analyzed by FC, dynamic light scattering (DLS), and atomic force microscopy (AFM). To generate biotin-streptavidin complexes, a biotinylated goat antimouse IgM antibody (Sigma-Aldrich, 5.5 mg/mL) and streptavidin-phycoerythrin (PE; R&D Systems, 10 μg/mL) were mixed at different ratios.

Detergent lysis

Triton X-100, Tween 20, sodium dodecyl sulfate, and Igepal-CA630 (all from Sigma-Aldrich) were used to lyse MPs and to disassemble ICs. A commercially available cell lysis buffer was also used (BD Biosciences). Various concentrations of the aforementioned detergents were mixed thoroughly with samples just before analyzing them by FC and DLS. For transmission electron microscopy (TEM) analysis, MPs were mixed with detergents and samples were centrifuged with 20 500*g* for 60 minutes. The pellets were fixed and embedded for TEM analysis.

TEM and immune EM

Shortly after centrifugation, the supernatants were carefully removed and the pellets were fixed at room temperature for 60 minutes with 4% paraformaldehyde in 0.01M PBS. After washing with PBS, the preparations were postfixed in 1% OsO_4 (Taab) for 30 minutes. After rinsing with distilled water, the pellets were dehydrated in graded ethanol, including block staining with 1% uranyl-acetate in 50% ethanol for 30 minutes, and embedded in Taab 812 (Taab). After overnight polymerization at 60°C and sectioning for EM, the ultrathin sections were analyzed with a Hitachi 7100 electron microscope equipped by Megaview II (lower resolution, Soft Imaging System) digital camera. For immune EM, after removal of the fixative and washing, the pellets were blocked with 4% bovine serum albumin in PBS for 60 minutes at room temperature and incubated with 1:1000 dilution of antihuman IgG-horseradish peroxidase (HRP) or antihuman IgM-HRP, respectively, at 4°C overnight (both from Sigma-Aldrich). After washing steps, 3,3-diaminobenzidine (Vector Laboratories) was applied as chromogen for visualization of ICs. Before osmification and embedding procedure, the pellets were washed in distilled water for 5 minutes. EM microphotographs were analyzed using ImageJ software (ImageJ 1.42q Wayne Rasband).

Atomic force microscopy

Using 2-beam interference method with the fourth harmonic of an Nd:YAG laser, gratings were fabricated on the surface of polycarbonate layers spin-coated onto Si wafers. Isolated MPs from blood plasma and SF were applied to the wafers with laser-structured surfaces. Incubation in the solutions lasted for 1 hour at 37°C, and then the wafers were washed 3 times in sterile distilled water on a horizontal shaker and finally allowed to dry overnight at room temperature. IC samples were seeded onto freshly cleaved mica. The surfaces were dried under a sterile air-flow cabinet for 30 minutes, then washed gently with sterile distilled water twice and allowed to dry overnight at room temperature. The AFM investigation of the topography of different biomolecule-covered surface structures was performed with tapping mode AFM (PSIA, serial no. XE-100) applying special TM AFM tips (type NSC15, MikroMasch) with nominal radius of curvature 10 nm, typical force constant of 40 N/m, and resonant frequency of 325 kHz. Both topography and shaded topography images were recorded using XEP1.5 (PSIA) acquisition software. Topography images were processed with XEI 1.6 (PSIA) using the Sobel Edge Enhancement method.

DLS analysis

DLS measurements were performed using an ALV goniometer (ALV) with a Melles Griot diode-pumped solid-state laser (CVI Melles Griot) at 457.5 nm wavelength (type 58 BLD 301). The intensity of the scattered light was measured at 90° and the autocorrelation function was calculated using an IBM PC-based data acquisition system developed in the Institute of Biophysics and Radiation Biology, Semmelweis University (Budapest, Hungary). Particle size distributions were determined by the maximum entropy method. The result is the relative contribution of the different-sized particles to the autocorrelation function. Because the scattered light intensity is strongly dependent on the size of the particles, this value does not only show the number of particles of a given radius but also overemphasizes those of larger size. Thus, minor amounts of large-sized impurities will have a significant contribution. We characterized the distribution using this value instead of the relative number of the particles because particle sizes in multicomponent systems are described properly by this function. The radius of the particles was calculated using sphere approximation.

Flow cytometry

Samples were analyzed using a FACSCalibur flow cytometer (BD Biosciences). The FC instrument settings and MP gating were adopted from previous works.[5,8,28] Microbeads of various sizes (4 μm and 400 nm in diameter from Invitrogen; 530 nm from Spherotech; 100 nm and 1 μm from Sigma-Aldrich) were used to select optimal instrument settings and MP gate.[29] The gate was established using 1 μm calibration beads as an upper right corner of the gate. The lower border was determined after assessing signal/noise ratios and positive event numbers. The gate was set in a way to exclude the highest possible noise but to detect the highest number of signal events. To reduce background event numbers, samples were diluted in 1:30 with 0.01 μm pore size membrane-filtered PBS or NaCl (Millipore). We used similarly filtered solutions used subsequently for all experiments of this study. Total event counts of MP and IC preparations were determined within the MP gate. To identify MPs, AX-FITC, AX-PE, anti-CD41a-FITC, anti-CD42a-peridinin chlorophyll protein, anti-CD68-FITC, and anti-CD45-peridinin chlorophyll protein-Cy5.5 were used (all purchased from BD Biosciences). AX staining was carried out in the presence of 2.5mM Ca^{2+}. Event numbers of equal sample volumes were counted for 30 seconds. Background fluorescence was compared with that of the isotype-control antibody. When detecting AX binding, 5mM ethylenediaminetetraacetic acid-containing 0.9% NaCl solution was used to determine the background fluorescence. Staining of ICs was carried out using antihuman IgM-FITC in 1:150 and antihuman IgG-FITC in 1:300 (both purchased from Sigma-Aldrich). Positive events were calculated within the MP gate, and the signal was compared with that of the isotype-control antibody.

Anti-C3 ELISA

To validate FC results, we performed an anti-C3 ELISA, a standard technique for the detection of ICs.[30] Briefly, antihuman C3 antibodies (Sigma-Aldrich) were coated onto polystyrene plates at a concentration of 0.2 μg/well. SF samples were used at 1:100 dilution (a concentration selected after preliminary experiments). Next, HRP-conjugated antihuman IgM and antihuman IgG (both from Sigma-Aldrich) were used at 1:50 000 and 1:30 000 dilutions, respectively. Orto-phenylene-diamine (Sigma-Aldrich) and hydrogen peroxide were added, and the absorbance was detected at 492 nm.

Fluorescence microscopy

The 20 500*g* pellet was obtained from SF samples of RA and OA patients (n = 3 in each group). To stain ICs in the pellet, it was diluted in 100 μL PBS and mixed with antihuman IgM-FITC or antihuman IgG-FITC, in 1:50 dilution. After 20-minute incubation at room temperature, samples were again centrifuged at 20 500*g* for 60 minutes. The pellet was fixed in 4% paraformaldehyde and applied onto slides. Coverslips were mounted on the slides and were analyzed by a Zeiss LSM 510 Meta confocal laser scanning microscope (Carl Zeiss). Slides were excited with a 488 nm Argon laser, and fluorescence was detected with a 505 to 570 nm BP filter.

Statistical analysis

SPSS software Version 15.0 was used for statistical analyses. Differences between RA and OA samples were analyzed by *t* test or Mann-Whitney test. For normality testing, one-sample Kolmogorov-Smirnov test was used. Correlations were analyzed by one-tailed Spearman test.

Results

Determination of the sizes of MPs

We used TEM and AFM to visualize MPs isolated from biologic samples. MPs are mostly spherical structures of various size and electron density as suggested by the TEM and AFM images (Figure 1A-B). We determined the sizes of MPs analyzing TEM and AFM images using ImageJ software (Version 1.42q). Based on the analysis of 180 vesicles, mean sizes (± SD) of blood plasma-derived MPs were found to be 182 ± 92 nm and 181 ± 71 nm by TEM and AFM, respectively (Figure 1C). Mean diameters of RA SF-derived vesicles were 234 ± 91 nm and 201 ± 78 nm as assessed by TEM and AFM images, respectively (Figure 1C). Both TEM and AFM have limitations of accuracy in determining MP sizes, as both methods examine nonfloating, pelleted, or solid surface-bound MPs. Therefore, next we selected DLS, suitable to study particle sizes in suspension. The mean (± SD) peak hydrodynamic radius of isolated MPs was 88 ± 10 nm (176 ± 20 nm in diameter, n = 3) in the case of healthy blood plasma, whereas it was 88 ± 15 nm (176 ± 30 nm in diameter, n = 3) in RA SF (Figure 1D). However, sizes of isolated MPs may also depend on the applied centrifugation and filtration processes. To test whether native, platelet-free plasma, and cell-free SF contain the same-sized floating MPs as pellets, we investigated the vesicle/particle size distributions in plasma and SF samples by DLS. We found peaks corresponding to MPs at approximately 80 to 90 nm (160-180 nm in diameter; Figure 1D). MP peaks were found at slightly smaller sizes in native samples than in the pelleted MP preparations (peak diameters were 173 ± 30 nm and 170 ± 44 nm in blood plasma and SF samples, respectively, n = 3 in each group). Moreover, SF and blood plasma also contained smaller particles, which were not present in the isolates. The TEM, AFM, and DLS results show concordantly that, in both native samples and isolated MP preparations, most MPs were within the size range of 80 to 400 nm irrespective of the source of the biologic sample.

Determination of sizes of ICs

Next, we tested size distributions of various ICs, including artificial and natural ones using AFM and DLS. AFM analysis of LF-anti-LF clearly showed irregular particles sized between 50 and 250 nm (Figure 2A). Based on the analysis of 180 particles, the mean diameter (± SD) was found to be 138 ± 46 nm (Figure 2B). We also tested ICs by DLS, a convenient method for IC size determination.[15] Total scattered light intensity in IC preparations was similar to that of MP preparations (data not shown). LF-anti-LF complex (antigen/antibody ratio 1:1) showed peaks at 6, 80, and 1000 nm radii (12, 160, and 2000 nm in diameter). OVA-anti-OVA complexes (1:1) revealed peaks at 3, 90, and 1000 nm radii (6, 180, and 2000 nm in diameter), whereas IgM-anti-IgM (1:1) resulted in peaks at 4 and 45 nm (8 and 90 nm in diameter; Figure 2C). All 3 artificial ICs showed peaks less than 10 nm in diameter, presumably corresponding to soluble ICs. The peaks at approximately 100 to 200 nm in diameter were considered as insoluble ICs overlapping with the sizes of MPs. The peaks above 1000 nm were considered as large IC precipitates.

We also tested whether not only artificial, but also natural (ex vivo) ICs, isolated from RA SFs, overlapped in size with MPs. IgG containing ICs showed peaks at 2, 105, and more than 1000 nm (4, 210, and 2000 nm diameter), whereas IgM ICs resulted in peaks at 6, 20, 105, and 1050 nm (12, 40, 210, and 2100 nm in diameter; Figure 2D). Thus, soluble and insoluble fractions as well as precipitates were detected within the isolates of natural ICs.

The soluble fraction of ICs was too small to interfere either with MP detection or isolation. On the contrary, the insoluble fraction (diameter range, 50-250 nm) overlaps with MP sizes (range, 80-400 nm). Precipitates do not overlap with MPs as they are usually above 1000 nm in diameter.

Detection of ICs by flow cytometry

To assess the consequences of shared size distribution and light-scattering properties of MPs and ICs, we tested whether ICs provided a signal within the commonly used MP gate in FC. Within

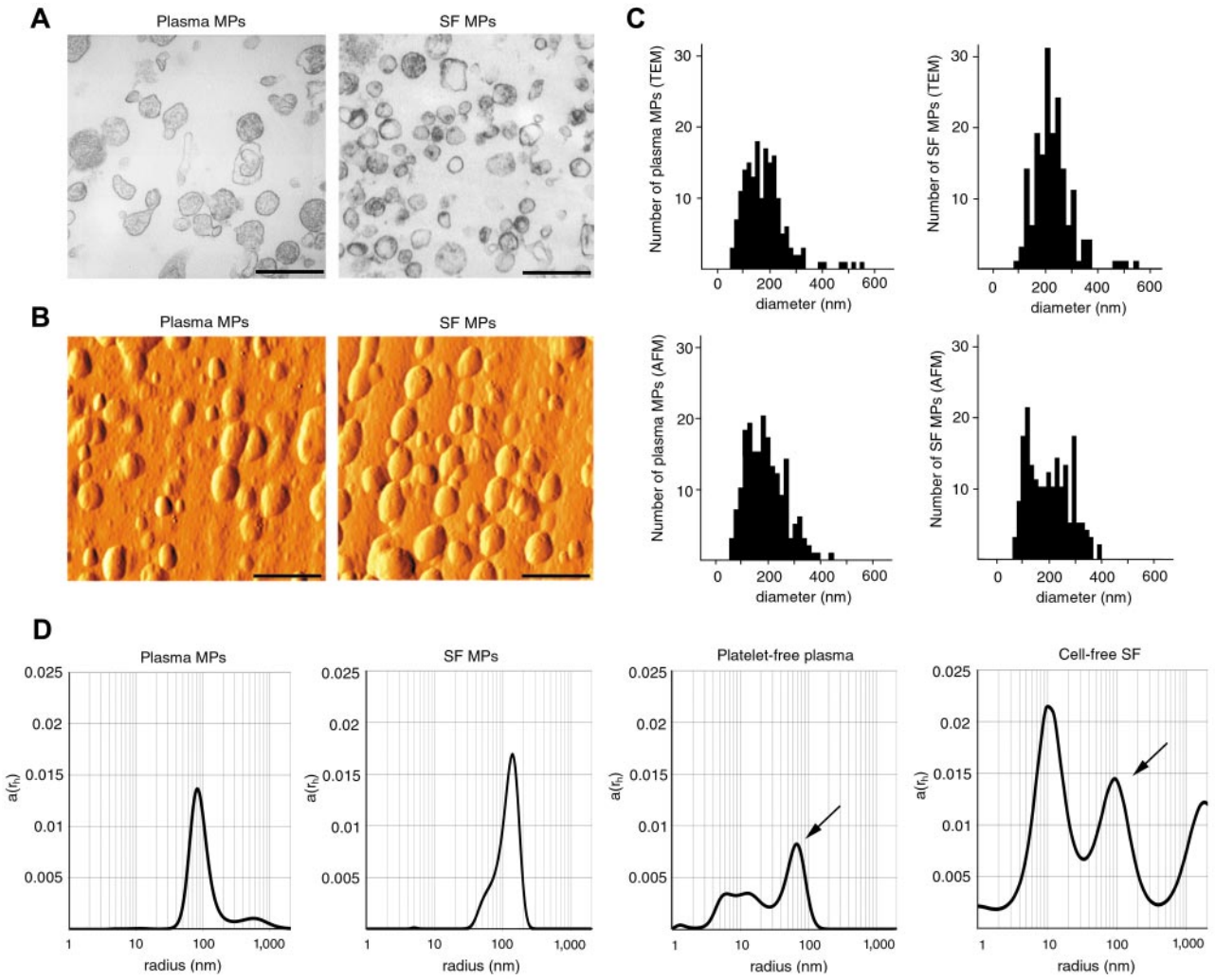

Figure 1. Size determination of MPs. (A) TEM images of healthy blood plasma- and RA SF-derived, isolated MPs. Original magnification × 50 000. Scale bars represent 500 nm. Images were recorded at room temperature using Hitachi 7100 electron microscope equipped with a Megaview II digital camera. (B) Shaded topography AFM images of healthy blood plasma- and RA SF-derived, isolated MPs. Scale bars represent 500 nm. Images were captured at room temperature using a PSIA XE-100 AFM with a XEP1.5 acquisition software. The imaging medium was air. Topography images were processed with XEI 1.6 software using the Sobel Edge Enhancement method. (C) MP size distributions, determined on the basis of TEM and AFM images of 180-180 MPs, are shown by histograms. For the analysis of particles, ImageJ software (Version 1.42q) was used. (D) Analysis of isolated MPs and native biologic samples by DLS. The x-axis is set to logarithmic scale; $a(r_h)$ denotes the coefficient of autocorrelation function of the scattered electric field. Arrows indicate peaks corresponding to MPs in the native samples. DLS experiments were carried out at 21°C.

this gate, MPs were clearly detected based on their AX binding and/or their cell-surface marker positivity (Figure 3A-B). First, artificial ICs were investigated by FC (Figure 3C) and resulted in intense signals within the MP gate. When one of the components of an IC (antimouse IgM) was labeled with FITC, an intense fluorescent signal was detected (Figure 3D). This provided further evidence in support that ICs were, indeed, specifically detectable within the MP gate. IC formation was dependent on the applied antigen/antibody ratio, and we obtained typical Heidelberg histograms showing optimal ratios (Figure 3E). We also detected fluorescent signals when testing natural ICs (isolated from RA SFs) stained with antihuman IgG or antihuman IgM (supplemental Figure 1, available on the *Blood* Web site; see the Supplemental Materials link at the top of the online article). Our data suggest that ICs may be detected by FC and characterized by light-scattering properties similar to those of MPs.

The presence of ICs affects detection of membrane vesicles by FC

To determine whether the presence of ICs affected the detection of MPs in biologic samples (in which MPs and ICs are present simultaneously), we first developed a simple method to discriminate between IC- and MP-related events by FC. Different concentrations of detergents, including Triton X-100, Tween 20, sodium dodecyl sulfate, and Igepal-CA630, were tested to assess the degree of MP lysis or IC disassembly. After the addition of 0.05% Triton X-100 to the sample, most of the AX or CD41a positive events disappeared (Figure 4A). Similar results were obtained for CD68, CD45, and CD42a stainings of MPs (data not shown). CD42a staining and AX binding were abolished at nearly the same concentrations of the detergents (supplemental Figure 2). Because anti-CD42a and AX bind to MPs by distinct mechanisms, this observation proves that detergents lysed MPs rather than abrogated the binding of antibody/AX. ICs showed significant immunopositivity, even after the addition of 0.05% Triton X-100 (Figure 4B; supplemental Figure 2). The presence of the other applied detergents, a standard commercial cell lysis buffer (BD Biosciences), or 3 cycles of freezing and thawing also differentiated ICs from MPs (data not shown). To prove that 0.05% Triton X-100 indeed lysed MPs, we captured TEM images of control and detergent-treated MPs (Figure 4C). After addition of detergent, only membrane fragments, but no vesicular structures, were observed (Figure 4C). Furthermore, using DLS, a marked decrease

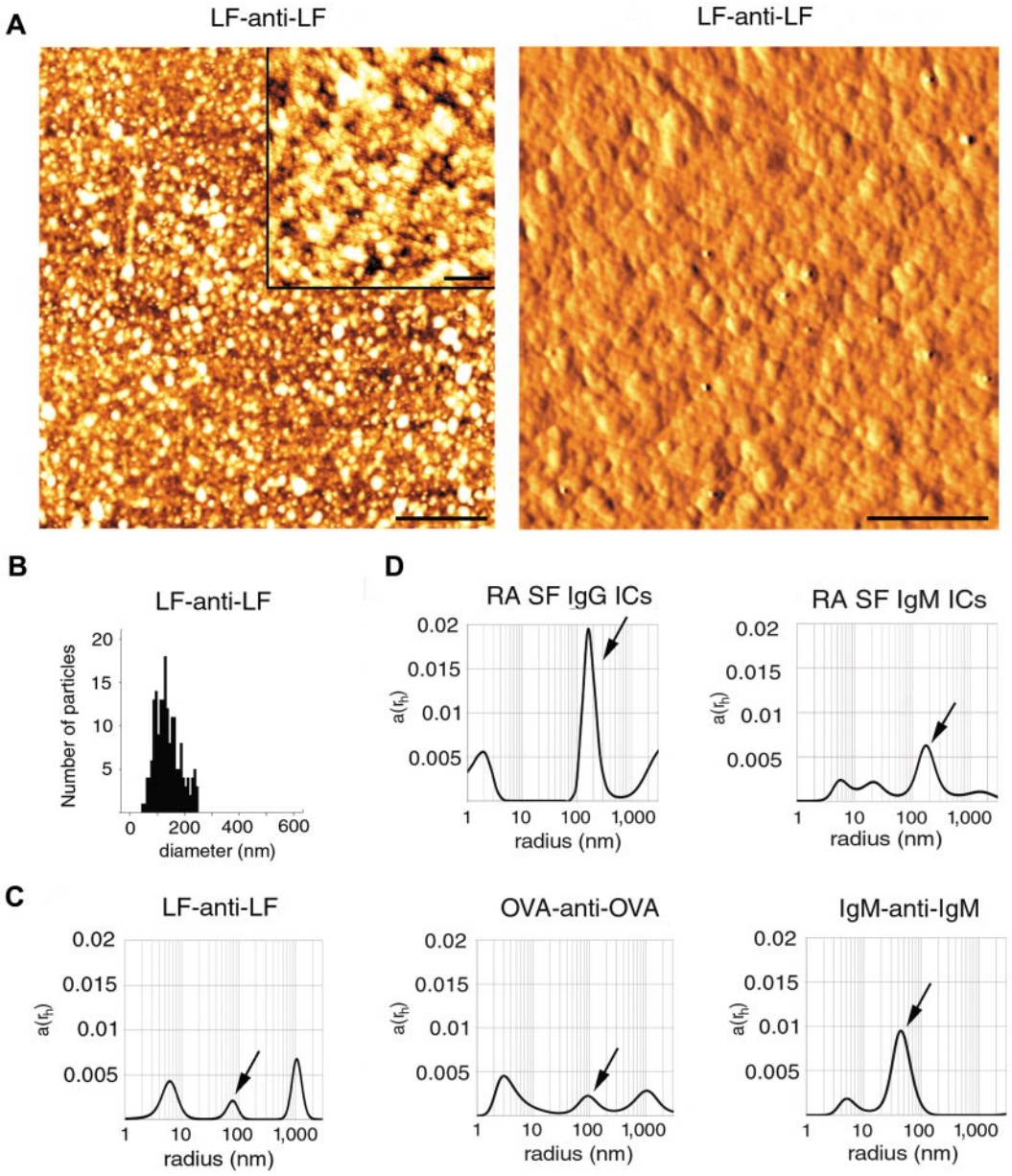

Figure 2. Size determination of ICs. (A) Topography (left panel) and shaded topography (right panel) AFM images of LF-anti-LF, artificial ICs. Scale bar represents 1 μm on the left panel. (Inset) Scale bar represents 200 nm. (Right panel) Scale bar represents 250 nm. Images were captured at room temperature using a PSIA XE-100 AFM with a XEP1.5 acquisition software. The imaging medium was air. Topography images were processed with XEI 1.6 software using the Sobel Edge Enhancement method. (B) The histogram represents particle size distribution. For the analysis of particles, ImageJ software (Version 1.42q) was used. (C) DLS analysis of LF-anti-LF, OVA-anti-OVA, IgM-anti-IgM ICs. Arrows indicate peaks overlapping with MP sizes. (D) RA SF ICs were isolated on an anti-IgG and anti-IgM agarose columns and were also analyzed by DLS. Arrows indicate peaks overlapping with MP sizes. The x-axis is set to logarithmic scale; $a(r_h)$ denotes the coefficient of autocorrelation function of the scattered electric field. DLS experiments were carried out at 21°C.

of the MP signal was detected after the addition of 0.05% Triton X-100 (Figure 4D). A remaining peak at a smaller size might have corresponded to membrane fragments also seen on TEM (Figure 4C). The decrease of the IC signal on the DLS plot was minimal after addition of the detergent (supplemental Figure 3). These experiments suggest that IC- or MP- related events can be discriminated using low concentrations of detergent: sensitive events correspond to MPs, whereas insensitive events reflect ICs or other protein complexes.

To exclude that ICs were bound to MP surfaces, we stained IC containing SF samples with antihuman IgG-FITC or antihuman IgM-FITC and AX-PE. Only minimal double staining was observed (Figure 4E), indicating that most MPs and ICs were present separately in RA SF. Immune EM images further confirmed that ICs were present in the space among MPs rather than on the surface of vesicles (see "ICs contaminate HP preparations").

To assess whether the presence of ICs in biologic samples affected routine MP enumeration by FC, diluted blood plasma and SF samples from RA and OA patients were stained with antihuman IgG-FITC and antihuman IgM-FITC. RA and OA plasma samples showed only minor positivity for ICs, making it unlikely that ICs affect MP counting in RA or OA blood plasma samples. On the contrary, RA SF samples showed extremely high positivity for ICs compared to OA samples (Figure 4F). All IgG and IgM events were resistant to 0.05% Triton X-100 lysis. To validate the system, we also used a conventional anti-C3 ELISA for the detection of ICs in SF samples. A strong correlation was found between FC and

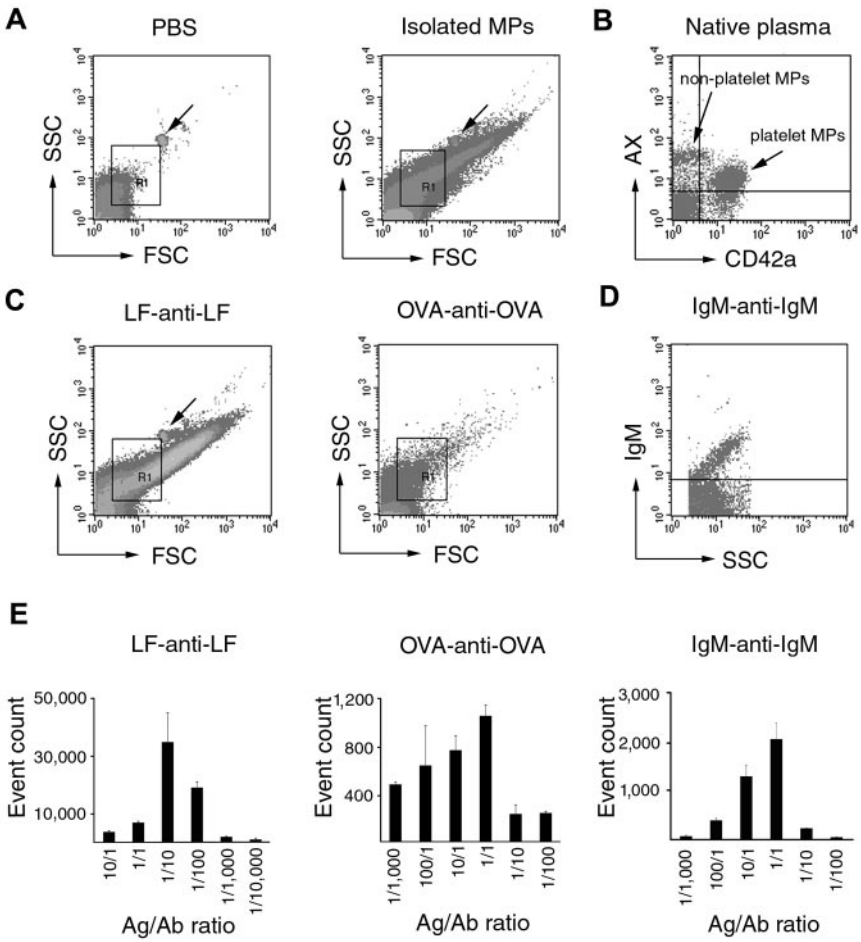

Figure 3. IC detection within the MP gate by FC. (A) Density plots showing PBS background and isolated MP preparation. Arrows indicate 1 μm calibration bead. R1 indicates the MP gate. (B) AX-PE- and CD42a-FITC-stained events within the MP gate from normal blood plasma. Two distinct populations can be recognized: an $AX^+/CD42a^+$ (platelet MPs) and an $AX^+/CD42a^-$ (non-platelet MPs) one. (C) Scatter plots of LF-anti-LF (1:10 ratio) IC and OVA-anti-OVA (1:1 ratio) IC. Arrow indicates 1 μm calibration bead. R1 indicates the MP gate. (D) Fluorescence intensity plot of mouse IgM-antimouse IgM-FITC (1:1) IC. Events are shown within the R1 gate. (E) The histograms show the effect of different antigen/antibody ratios on LF-anti-LF, OVA-anti-OVA, and IgM-antimouse IgM-FITC IC formation. The y-axes represent total event counts within the MP gate.

ELISA results regarding IgM ICs (one-tailed Spearman correlation, n = 22, rho = 0.48, $P = .01$), but not for IgG ICs (n = 22, rho = −0.23, $P = .14$) (supplemental Figure 4). This was probably because of the presence of rheumatoid factor (RF), an anti-IgG antibody, in the SF samples. RF may bind to the detection antibody in FC, thus, resulting in artificial ICs.

We tested the extent by which the high level of ICs affected the quantitative assessment of MPs in RA and OA SFs. Total event counts of SFs within the MP gate correlated with AX-, IgG-, and IgM-positive events (Table 1). In OA samples, total event counts strongly correlated with AX-positive but not with IC counts as the latter were absent in OA samples. Strikingly, in RA SFs, total event counts did not correlate with AX-positive MP event counts but showed strong correlation with those of ICs. These data suggest that in RA SFs total event counts depended on IC counts rather than on the amount of MPs. Hence, when enumeration of MPs is based on total event counts rather than on the detection of AX-positive events, FC data may lead to false results in samples containing high amounts of ICs. In line with this concept, we observed 1.41-fold elevation in the total event counts in RA compared with OA SF samples (n = 21, $P = .147$, *t* test after normality testing), whereas there was only a 1.25-fold increase in the AX-positive events (n = 21, $P = .359$, *t* test) (Figure 4F). As a conclusion, in this system, total event counts overestimated the real MP counts because of the highly elevated IC content.

Importantly, IC formation may falsify MP detection by FC in systems that ignore the potential presence of ICs. We observed that, using indirect immune labeling, primary and secondary antibodies also form ICs detectable within the MP gate (supplemental Figure 5A). These events could not be diminished by the use of low concentration of detergent (0.05% Triton X-100, data not shown). We also assessed whether streptavidin-PE and a biotinylated antibody could form complexes detectable by FC within the MP gate. As avidin is a homotetramer and a biotinylated antibody usually carries 3 to 6 molecules of biotin,[31] the streptavidin-biotinylated antibody complexes gave MP-mimicking fluorescent signals at an optimal ratio (supplemental Figure 5A).

Moreover, antibodies tend to aggregate, and self-aggregation of an antibody may also lead to false signals. There are several factors that induce self-aggregation of an antibody, including protein concentration, temperature, ionic strength, pH, and agitation.[32,33] We investigated the effect of agitation: a 30-second vortexing of a CD14-PE (BD Biosciences) antibody in either PBS or normal blood plasma resulted in the appearance of a new, fluorescent event group at the SSC-FL1 plot (supplemental Figure 5B). These events could not be abolished after the addition of low concentrations of detergents (0.05% Triton X-100; supplemental Figure 5B).

ICs contaminate MP preparations

We have shown that ICs may confound FC detection and enumeration of MPs. The next issue we investigated was whether ICs were present in conventionally isolated MP preparations. MPs were pelleted at 20 500*g* for 60 minutes as described earlier.[25,26] The 20 500*g* pellets were labeled with antihuman IgM-FITC and antihuman IgG-FITC and analyzed by fluorescence microscopy. A marked difference was observed between OA and RA sample-derived pellets (Figure 5A). On the basis of our FC data, we hypothesized that the fluorescent staining in the MP pellet corresponded to ICs. To exclude that MPs were

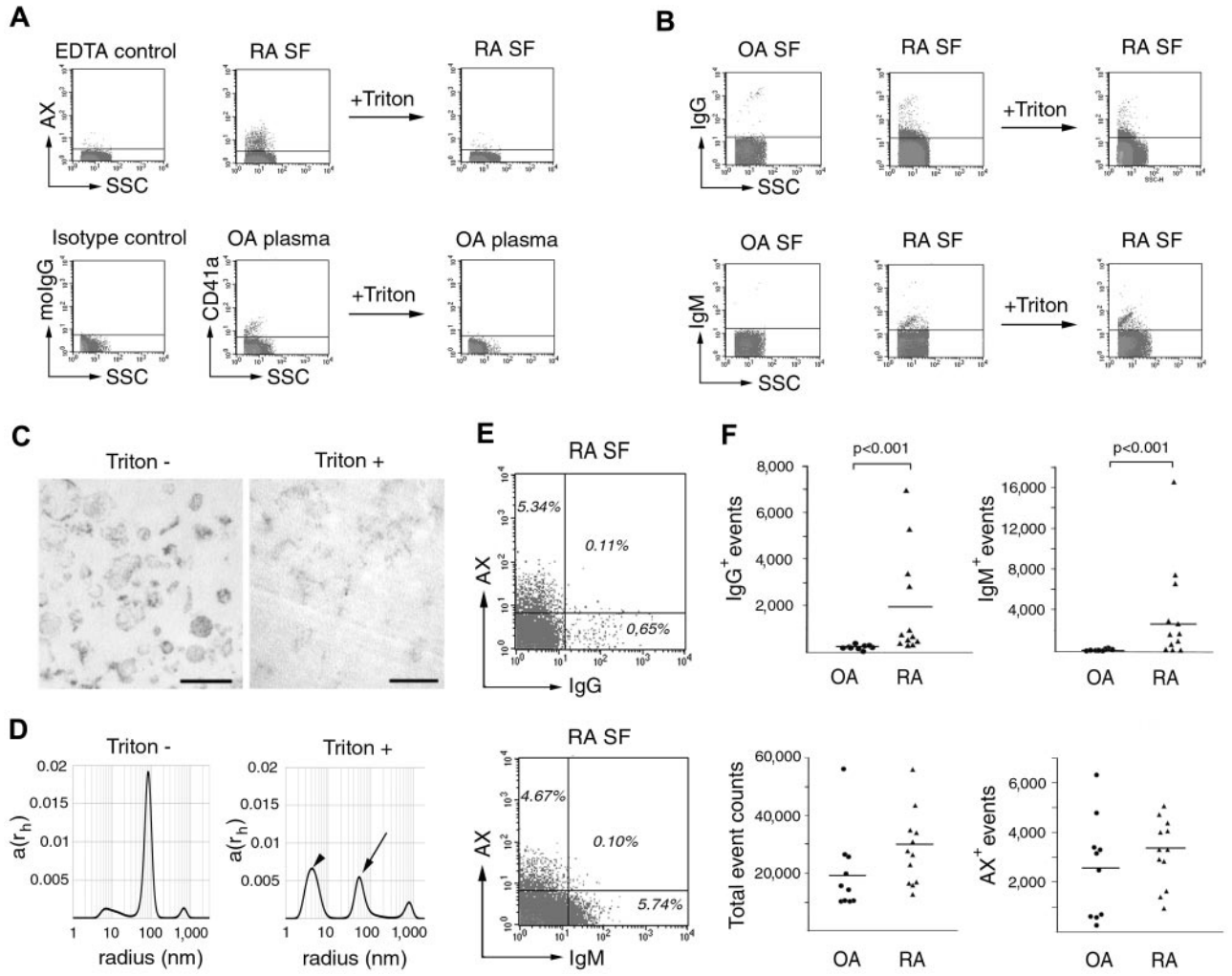

Figure 4. FC analysis of MP and IC containing samples. (A) MPs from RA SF and OA plasma have been stained with AX-FITC or CD41a-FITC and were subjected to detergent lysis by 0.05% Triton X-100. moIgG denotes antimouse IgG used for isotype control. (B) SFs from OA and RA patients were stained with anti-IgG-FITC or anti-IgM-FITC and were also subjected to detergent lysis by 0.05% Triton X-100. All plots represent events from the MP gate. (C) To prove MP lysis, isolated MPs were visualized by TEM before and after lysis. Original magnification × 20 000. Scale bars indicate 400 nm. Images were captured at room temperature using Hitachi 7100 electron microscope equipped with a Megaview II digital camera. (D) DLS of MPs before and after addition of detergent. The x-axis is set to logarithmic scale; $a(r_h)$ denotes the coefficient of autocorrelation function of the scattered electric field. Arrow indicates the remaining MP-related signal. Arrowhead indicates the signal of Triton X-100. DLS experiments were carried out at 21°C. (E) Dot plots of RA SFs stained with AX-PE and anti-IgG-FITC or anti-IgM-FITC (n = 3 in each group). Events are shown within the R1 gate. (F) IgG^+, IgM^+, total, and AX^+ event counts within the MP of RA and OA SFs. Horizontal lines indicate mean values. The *P* values were obtained from Mann-Whitney test (n = 21).

stained by the antihuman IgM or antihuman IgG antibodies, we conducted immune TEM analysis. Among the clearly recognizable MPs, amorphous structures showed immunopositivity, indicating the presence of ICs within the pellet (Figure 5B). The majority of MPs were not stained by the antibodies in line with the previous FC analysis (Figure 4E). Subsequent FC and DLS also proved the presence of ICs in the 20 500*g* pellet, whereas the 20 500*g* supernatants contained substantially fewer immunopositive events (Figure 5C-D). Of note, in the pellets, peaks smaller than 50 nm were also detected by DLS, probably corresponding to resolubilizing insoluble ICs. In summary, these results confirmed that ICs indeed were simultaneously sedimented with MPs in the 20 500*g* pellet.

Table 1. Correlations of total event counts and AX^+/IgG^+/IgM^+ event counts by FC

Total event count	AX^+ events	IgG^+ events	IgM^+ events	AX^++IgG^+ +IgM^+ events
RA + OA	0.634*	0.716†	0.515*	0.848†
OA	0.883*	0.383	−0.510	0.867*
RA	0.154	0.930†	0.720*	0.748*

Values indicate correlation coefficients obtained from one-tailed Spearman correlations.

*$P < .01$.

†$P < .001$.

Discussion

Over the last decades, understanding of the universal formation of membrane vesicles by prokaryotic[34] and eukaryotic[35] cells has challenged the long existing paradigm of intercellular communication. The explosion-like rise in the number of publications using predominantly flow cytometric platforms to analyze microvesicles/MPs in patient-derived samples has raised concerns about the reliability of this technology as it may conceal pitfalls that lead to erratic conclusions.

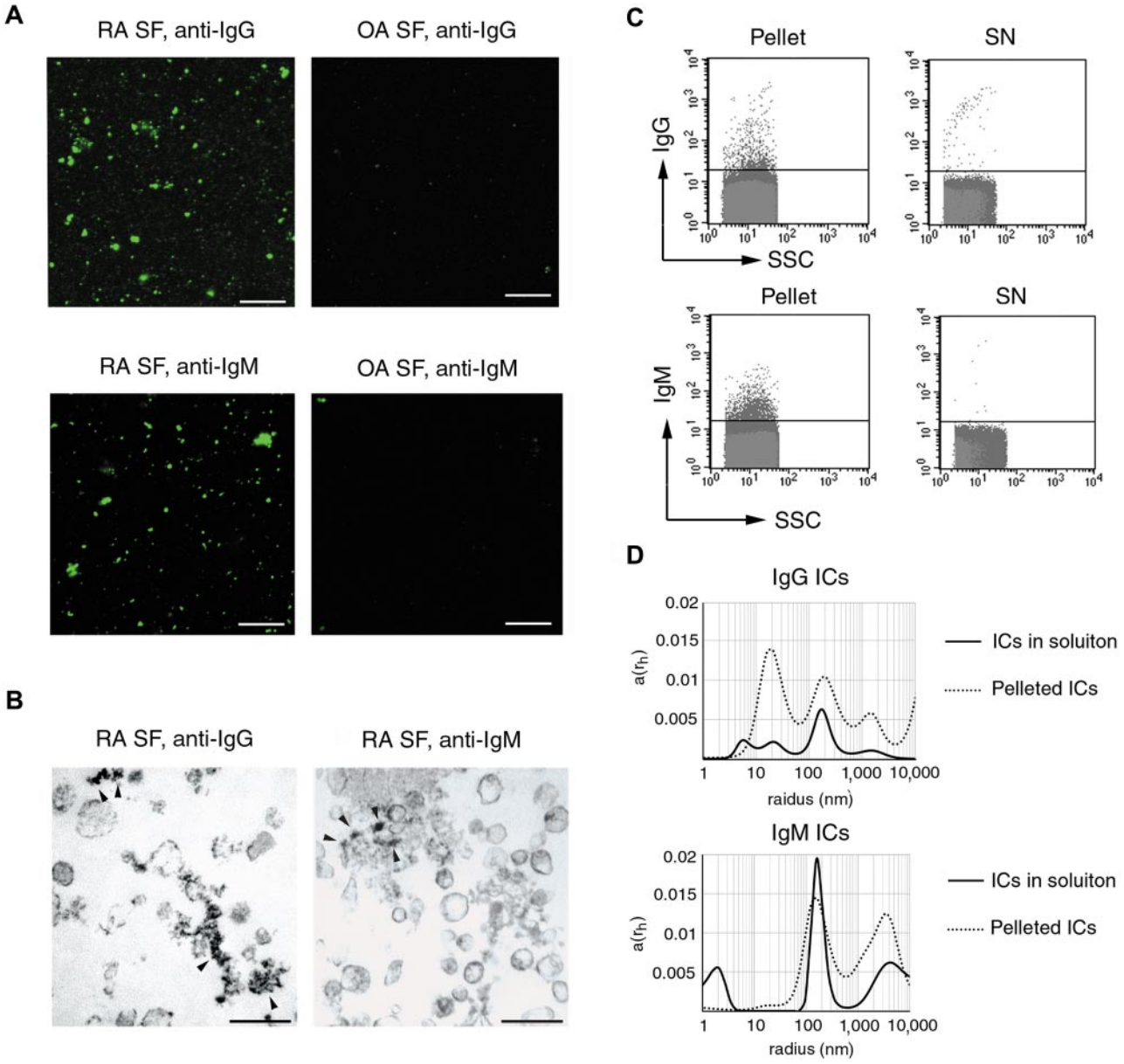

Figure 5. Cosedimentation of ICs and MPs. (A) Fluorescent microscopy images of antihuman IgG-FITC or antihuman IgM-FITC-stained 20 500*g* pellets from RA and OA SFs. Images were captured at room temperature using a Zeiss LSM 510 Meta confocal laser scanning microscope equipped with an inverted Axiovert 200M microscope, 63× Plan Apochromat oil immersion differential interference contrast objectives (numerical aperture, 1.4). The acquisition software was AIM LSM, Version 4.2. (B) The 20 500*g* pellet from RA SF was analyzed by immune EM, stained with antihuman IgG-HRP or antihuman IgM-HRP. Arrowheads indicate immunopositive structures among MPs. Original magnification × 50 000. Scale bar represents 400 nm. Images were captured at room temperature using Hitachi 7100 electron microscope equipped with a Megaview II digital camera. (C) FC analysis revealed that isolated ICs were present in the pellet and were nearly absent in the supernatant (SN). (D) Isolated IgG or IgM ICs from RA SFs were also analyzed by DLS. The x-axis is set to logarithmic scale; $a(r_h)$ denotes the coefficient of autocorrelation function of the scattered electric field. DLS experiments were carried out at 21°C.

In this work, we addressed basic questions regarding MPs. We were the first to compare 3 different methodologies and analyze the size distributions of human blood plasma and SF-derived MPs using TEM, AFM, and DLS. The 3 methods resulted in highly concordant results concerning the size distribution of a given MP preparation. However, TEM and AFM slightly overestimated mean vesicle sizes compared with DLS. This could be explained by the fact that, because of sedimentation, the morphology, shape, and consequently the size of vesicles in the pellet might be altered compared with MPs floating in biologic fluids. Our analysis of blood plasma and SF revealed that most MPs had diameters between 80 and 400 nm. In native MP-containing biologic samples, we detected peaks similar to those obtained when analyzing isolated MPs. However, the isolated (pelleted) MPs were somewhat bigger than those in the native samples. This could be the result of either the fusion of some vesicles during centrifugation or a higher efficacy to pellet out vesicles of larger size. In native samples, peaks smaller than 100 nm were also detected by DLS, probably corresponding to exosomes, lipoproteins, or smaller protein complexes. The size of low-density lipoprotein diameters is reported to be in between 25 and 27 nm,[36] high-density lipoprotein particles are approximately 10 nm in diameter,[37] whereas triglyceride-rich particles have a diameter around 40 to 80 nm.[38] Because of their size range, lipoproteins usually do not interfere with MP measurements. Previous reports documented a mean MP size of 247 to 289 nm without filtration in fresh-frozen plasma[13] and a peak diameter for red blood cell microvesicles of 179 nm.[39]

Analyzing ICs, we found shared biophysical properties with MPs. Using DLS and AFM, we found that ICs contained a fraction overlapping in size with MPs. FC and DLS analyses revealed MPs and ICs were characterized by similar light-scattering properties. Concerning the size, previous reports described insoluble ICs with 200 and 220 nm radii[15,40] overlapping with MP size distributions that we determined in our experimental systems. In contrast to insoluble ICs, soluble ICs and precipitates do not share biophysical parameters with MPs, being far below and well above the MP size range, respectively. Of note, it is highly unlikely that ICs would also interfere with exosome-related studies if exosomes are purified using ultracentrifugation followed by a subsequent sucrose density gradient ultracentrifugation: exosomes are found at lower densities (1.13-1.19 g/mL)[1] compared with ICs and aggregated IgG (> 1.20 g/mL).[41]

A rapidly growing body of FC data report MP analyses of patient-derived samples in a broad variety of diseases. We hypothesized that the shared parameters of MPs and ICs might have led to spurious findings in the field. These findings prompted us to develop a simple novel method to discriminate MPs from ICs. Using detergent lysis, our data show that, in biologic samples, in which ICs are abundant, total event counts within the MP gate probably predict IC rather the real MP content.

Results, obtained without MP-IC discrimination, should be interpreted cautiously. This is also underlined by a previous work in which RA SF MPs were reported to carry IgG, IgM, complement components, serum amyloid P and C-reactive protein.[42] Without AX staining, based only on immunopositivity within the MP gate, the authors reported that in MP preparations from RA SF, total event counts, IgG, IgM, C1q, C3, C4, C-reactive protein, and serum amyloid P reactivities were elevated compared with control SFs, RA, and healthy plasma samples. All of the aforementioned molecules are either components of or are associated with ICs[43,44]; therefore, this study presumably detected and described ICs rather than MPs. In our work, we found that in biologic fluids MPs and insoluble ICs appear as distinct particles.

Our findings have also broader consequences. Indirect immunolabeling, avidin-biotin complexes, and the self-aggregation of an antibody may also lead to MP-mimicking signals, which are detergent resistant. Of importance, the overlapping parameters of ICs and MPs may also affect the purity of isolated MP preparations. Most workgroups apply differential-centrifugation protocols to prepare MPs. In this study, we show that both artificial and natural ICs may contaminate the so-called "MP pellet." Consistent with our findings, a recent report has documented the presence of proteinaceous contamination in urinary microvesicle preparations.[45] Given the well-known ability of ICs to provoke robust biologic responses,[16,17] functional assays that use MPs isolated by differential centrifugation may lead to misleading results. Therefore, for functional assays of MPs, AX or other surface marker-based affinity isolation is highly recommended.[46,47]

Our findings also have relevance to nonrheumatologic diseases, such as acute coronary syndrome and sickle cell disease in which the presence of circulating ICs is well documented[48,49] and may cause interference with MP detection.

Data, presented here, bring attention to the substantial size overlap between MPs and ICs that may falsify both detection results and functional assays of MPs. Whether these findings also imply that in vivo MPs may penetrate and deposit tissue spaces described previously to be accessible for ICs remains to be answered.

Acknowledgments

The authors thank Attila Cselenyák and Fluorescent Technics Core Facility (Institute of Human Physiology and Clinical Experimental Research, Semmelweis University, Budapest, Hungary) for the assistance in fluorescent microscopy.

This work was supported by the Semmelweis Foundation (grants OTKA K 73247, OTKA 77537, and Kerpel-Fronius Ödön Fellowship) and Baross Gábor (REG-KM-09-1-2009-0010). G.N. is a Bolyai Research Fellow.

Authorship

Contribution: E.I.B. designed research; B.G., K.M., K.P., M.P., and P.M. performed research; B.G., K.M., K.P., M.P., P.M., M.A.D., Á. Sipos, A. Szalai, A.P., K.T., M.C., and Á.K. collected data; B.G., K.M., É.P., and E.I.B. analyzed data; B.G., É.P., G.N., S.G., A.F., and E.I.B. interpreted data; K.M., M.A.D., Á. Sipos, A. Szalai, I.V., M.C., and Á.K. contributed vital analytical tools; and B.G. and E.I.B. wrote the manuscript.

Conflict-of-interest disclosure: The authors declare no competing financial interests.

Correspondence: Edit I. Buzás, Nagyvárad tér 4, H-1089 Budapest, Hungary; e-mail: edit.buzas@gmail.com.

References

1. Théry C, Ostrowski M, Segura E. Membrane vesicles as conveyors of immune responses. *Nat Rev Immunol.* 2009;9(8):581-593.
2. Distler JH, Pisetsky DS, Huber LC, Kalden JR, Gay S, Distler O. Microparticles as regulators of inflammation: novel players of cellular crosstalk in the rheumatic diseases. *Arthritis Rheum.* 2005; 52(11):3337-3348.
3. Orozco AF, Lewis DE. Flow cytometric analysis of circulating microparticles in plasma. *Cytometry A.* 2010;77(6):502-514.
4. Smalley DM, Sheman NE, Nelson K, Theodorescu D. Isolation and identification of potential urinary microparticle biomarkers of bladder cancer. *J Proteome Res.* 2008;7(5):2088-2096.
5. Boilard E, Nigrovic PA, Larabee K, et al. Platelets amplify inflammation in arthritis via collagen-dependent microparticle production. *Science.* 2010;327(5965):580-583.
6. Messer L, Alsaleh G, Freyssinet JM, et al. Microparticle-induced release of B-lymphocyte regulators by rheumatoid synoviocytes. *Arthritis Res Ther.* 2009;11(2):R40.
7. Bernal-Mizrachi L, Jy W, Jimenez JJ, et al. High levels of circulating endothelial microparticles in patients with acute coronary syndromes. *Am Heart J.* 2003;145(6):962-970.
8. Sellam J, Proulle V, Jüngel A, et al. Increased levels of circulating microparticles in primary Sjögren's syndrome, systemic lupus erythematosus and rheumatoid arthritis and relation with disease activity. *Arthritis Res Ther.* 2009;11(5):R156.
9. Ghosh AK, Secreto CR, Knox TR, Ding W, Mukhopadhyay D, Kay NE. Circulating microvesicles in B-cell chronic lymphocytic leukemia can stimulate marrow stromal cells: implications for disease progression. *Blood.* 2010;115(9): 1755-1764.
10. Toth B, Liebhardt S, Steinig K, et al. Platelet-derived microparticles and coagulation activation in breast cancer patients. *Thromb Haemost.* 2008;100(4):663-669.
11. Beyer C, Pisetsky DS. The role of microparticles in the pathogenesis of rheumatic diseases. *Nat Rev Rheumatol.* 2010;6(1):21-29.
12. Dignat-George F, Freyssinet JM, Key NS. Centrifugation is a crucial step impacting microparticle measurement. *Platelets.* 2009;20(3):225-226; author reply 227-228.
13. Lawrie AS, Albanyan A, Cardigan RA, Mackie IJ, Harrison P. Microparticle sizing by dynamic light scattering in fresh-frozen plasma. *Vox Sang.* 2009;96(3):206-212.
14. Robert S, Poncelet P, Lacroix R, et al. Standardization of platelet-derived microparticle counting using calibrated beads and a Cytomics FC500 routine flow cytometer: a first step towards multicenter studies? *J Thromb Haemost.* 2009;7(1): 190-197.

15. Khlebtsov BN, Burygin GL, Matora LY, Shchyogolev SY, Khlebtsov NG. A method for studying insoluble immune complexes. *Biochim Biophys Acta.* 2004;1670(3):199-207.
16. Jancar S, Sánchez Crespo M. Immune complex-mediated tissue injury: a multistep paradigm. *Trends Immunol.* 2005;26(1):48-55.
17. Silverman GJ, Carson DA. Roles of B cells in rheumatoid arthritis. *Arthritis Res Ther.* 2003; 5[suppl 4]:S1-S6.
18. Davies KA. Michael Mason Prize Essay 1995: complement, immune complexes and systemic lupus erythematosus. *Br J Rheumatol.* 1996; 35(1):5-23.
19. Cohen SD, Kimmel PL. Immune complex renal disease and human immunodeficiency virus infection. *Semin Nephrol.* 2008;28(6):535-544.
20. Beneduce L, Castaldi F, Marino M, et al. Squamous cell carcinoma antigen-immunoglobulin M complexes as novel biomarkers for hepatocellular carcinoma. *Cancer.* 2005;103(12):2558-2565.
21. Gropp C, Havemann K, Scherfe T, Ax W. Incidence of circulating immune complexes in patients with lung cancer and their effect on antibody-dependent cytotoxicity. *Oncology.* 1980; 37(2):71-76.
22. Fennelly DW, Norton L, Sznol M, Hakes TB. A phase II trial of extracorporeal plasma immunoadsorption of patient plasma with PROSORBA columns for treating metastatic breast cancer. *Cancer.* 1995;75(8):2099-2102.
23. Marcello A, Wirths O, Schneider-Axmann T, Degerman-Gunnarsson M, Lannfelt L, Bayer TA. Circulating immune complexes of Abeta and IgM in plasma of patients with Alzheimer's disease. *J Neural Transm.* 2009;116(7):913-920.
24. Arnett FC, Edworthy SM, Bloch DA et al. The American Rheumatism Association 1987 revised criteria for the classification of rheumatoid arthritis. *Arthritis Rheum.* 1988;31:315-324.
25. Leroyer AS, Rautou PE, Silvestre JS, et al. CD40 ligand+ microparticles from human atherosclerotic plaques stimulate endothelial proliferation and angiogenesis a potential mechanism for intraplaque neovascularization. *J Am Coll Cardiol.* 2008;52(16):1302-1311.
26. Biró É, Nieuwland R, Sturk A. Measuring circulating cell-derived microparticles. *J Thromb Haemost.* 2004;2:1843-1844.
27. Glant TT, Mikecz K, Roughley PJ, Buzás E, Poole AR. Age-related changes in protein-related epitopes of human articular-cartilage proteoglycans. *Biochem J.* 1986;236(1):71-75.
28. Aras O, Shet A, Bach RR, et al. Induction of microparticle- and cell-associated intravascular tissue factor in human endotoxemia. *Blood.* 2004; 103(12):4545-4553.
29. Pap E, Pállinger E, Falus A, et al. T lymphocytes are targets for platelet- and trophoblast-derived microvesicles during pregnancy. *Placenta.* 2008; 29(9):826-832.
30. Stanilova SA, Slavov ES. Comparative study of circulating immune complexes quantity detection by three assays: CIF-ELISA, C1q-ELISA and anti-C3 ELISA. *J Immunol Methods.* 2001;253(1): 13-21.
31. Haugland RP, You WW. Coupling of monoclonal antibodies with biotin. *Methods Mol Biol.* 1995;45: 223-233.
32. Cromwell ME, Hilario E, Jacobson F. Protein aggregation and bioprocessing. *AAPS J.* 2006;8(3): E572-E579.
33. Fesinmeyer RM, Hogan S, Saluja A, et al. Effect of ions on agitation- and temperature-induced aggregation reactions of antibodies. *Pharm Res.* 2009;26(4):903-913.
34. Post DM, Zhang D, Eastvold JS, Teghanemt A, Gibson BW, Weiss JP. Biochemical and functional characterization of membrane blebs purified from Neisseria meningitidis serogroup B. *J Biol Chem.* 2005;280(46):38383-38394.
35. Oliveira DL, Freire-de-Lima CG, Nosanchuk JD, Casadevall A, Rodrigues ML, Nimrichter L. Extracellular vesicles from Cryptococcus neoformans modulate macrophage functions. *Infect Immun.* 2010;78(4):1601-1609.
36. Tsukamoto H, Takei I, Ishii K, Watanabe K. Simplified method for the diameter sizing of serum low-density lipoprotein using polyacrylamide gradient gel electrophoresis. *Clin Chem Lab Med.* 2004;42(9):1009-1012.
37. Cavigiolio G, Shao B, Geier EG, Ren G, Heinecke JW, Oda MN. The interplay between size, morphology, stability, and functionality of high-density lipoprotein subclasses. *Biochemistry.* 2008;47(16):4770-4779.
38. Lu S, Yao Y, Cheng X, et al. Overexpression of apolipoprotein A-IV enhances lipid secretion in IPEC-1 cells by increasing chylomicron size. *J Biol Chem.* 2006;281(6):3473-3483.
39. Salzer U, Hinterdorfer P, Hunger U, Borken C, Prohaska R. Ca(++)-dependent vesicle release from erythrocytes involves stomatin-specific lipid rafts, synexin (annexin VII), and sorcin. *Blood.* 2002;99(7):2569-2577.
40. Gorgani NN, Easterbrook-Smith SB, Altin JG. The formation of insoluble immune complexes between ovalbumin and anti-ovalbumin IgG occurs in at least two distinct phases dependent on reactant concentration and ionic strength. *Biochim Biophys Acta.* 1996;1317(1):45-54.
41. Rødahl E, Iversen OJ, Dalen AB. Preparative isolation of immune complexes from serum by sucrose gradient ultracentrifugation. *Scand J Immunol.* 1984;20(1):21-26.
42. Biró E, Nieuwland R, Tak PP, et al. Activated complement components and complement activator molecules on the surface of cell-derived microparticles in patients with rheumatoid arthritis and healthy individuals. *Ann Rheum Dis.* 2007; 66(8):1085-1092.
43. Agrawal A, Radha HB, Cropsey CL, Suresh MV, Singh SK. C-reactive protein binds to immune complexes. *FASEB J.* 2008;22:673-679.
44. Brown MR, Anderson BE. Receptor-ligand interactions between serum amyloid P component and model soluble immune complexes. *J Immunol.* 1993;151(4):2087-2095.
45. Rood IM, Deegens JK, Merchant ML, et al. Comparison of three methods for isolation of urinary microvesicles to identify biomarkers of nephrotic syndrome. *Kidney Int.* 2010;78(8):810-816.
46. Bianco F, Pravettoni E, Colombo A, et al. Astrocyte-derived ATP induces vesicle shedding and IL-1 beta release from microglia. *J Immunol.* 2005;174(11):7268-7277.
47. Théry C, Amigorena S, Raposo G, Clayton A. Isolation and characterization of exosomes from cell culture supernatants and biologic fluids. *Curr Protoc Cell Biol.* 2006;Chapter 3:Unit 3.22.
48. Mustafa A, Nityanand S, Berglund L, Lithell H, Lefvert AK. Circulating immune complexes in 50-year-old men as a strong and independent risk factor for myocardial infarction. *Circulation.* 2000;102(21):2576-2581.
49. Anyaegbu CC, Okpala IE, Aken'ova AY, Salimonu LS. Complement haemolytic activity, circulating immune complexes and the morbidity of sickle cell anaemia. *APMIS.* 1999;107(7):699-702.